ChemCatChem

The European Society Journal for Catalysis

Chemistry Europe

European Chemical Societies Publishing

Supported by GECATS GERMAN CATALYSIS SOCIETY

Accepted Article

Title: Enhancing CO2 Reduction Efficiency on Cobalt Phthalocyanine via Axial Ligation

Authors: Hongxing Kang, Aaliyah Staples-West, Audrey Washington, Chris Turchiano, Andrew Cooksy, Jier Huang, and Jing Gu

To be cited as: *ChemCatChem* **2023**, e202300576

Link to VoR: https://doi.org/10.1002/cctc.202300576

WILEY VCH

10.1002/cctc.202300576

WILEY-VCH

RESEARCH ARTICLE

Enhancing CO_2 Reduction Efficiency on Cobalt Phthalocyanine via Axial Ligation

Hongxing Kang, [a] Aaliyah Staples-West,[a] Audrey Washington,[a] Chris Turchiano,[a] and Andrew Cooksy,[a] Jier Huang,[b] and Jing Gu*[a]

[a] Hongxing Kang, Aaliyah Staples-West, Audrey Washington, Chris Turchiano, Prof. Andrew Cooksy, Prof. Jing Gu
Department of Chemistry and Biochemistry
San Diego State University
5500 Campanile Drive, San Diego, CA 92182, United States
E-mail: jgu@sdsu.edu
[b] Prof. Jier Huang
Department of Chemistry
Marquette University,
Milwaukee, WI, 53201, United States

Supporting information for this article is given via a link at the end of the document.

Abstract: Electrochemical reduction of carbon dioxide (CO_2RR) to value-added products is a promising strategy to alleviate the greenhouse gas effect. Molecular catalysts, such as cobalt (II) phthalocyanine (CoPc), are known to be efficient electrocatalysts that are capable of converting CO_2 into carbon monoxide (CO). Herein, we report an axial modification strategy to enhance CoPc's CO_2RR performance. After coordinating with axial ligands, the electron density of Co was depleted via π-backbonding. This π-backbonding weakened the Co-CO bond, resulting in rapid desorption of CO. Also, the presence axial ligands elevated the Co dz^2 orbital energy, resulting in a significantly enhanced CO_2 selectivity, evidenced by an increased faradaic efficiency (FE) from 82% (CoPc) to 91% (pyridine) and 94% (imidazole) at -0.82 V vs. RHE. Density functional theory calculations reveal that axial ligation of CoPc can reduce the energy barrier for CO_2 activation and facilitate the formation of *COOH.

Introduction

Effective conversion of carbon dioxide(CO_2) to value-added products is an attractive strategy to alleviate global warming by reducing atmospheric CO_2 concentration while providing renewable pathways to address long-term seasonal energy shortage and chemical production.[1] Electrochemical reduction of CO_2 has gained significant interest as it is a sustainable approach that operates under ambient conditions and is driven by renewable energy sources, such as wind and solar energy.[2] However, the progress of carbon dioxide reduction reaction (CO_2RR) is currently hindered by the lack of cost-effective catalysts with satisfactory efficiency, selectivity, and long-term stability.[3]

Metal complexes with abundant redox-active sites for CO_2 adsorption and activation have attracted substantial attention.[4] Among them, transition metal phthalocyanines with a tunable coordination structure and well-defined catalytic active site are deemed to be promising molecular catalysts,[5] especially cobalt phthalocyanine (CoPc).[6] For example, previous work showed that the efficiency and selectivity of CoPc can be accelerated by modifying its peripheral functional substituents to fine-tune the electron density of the metal center.[7] Alternatively, immobilized CoPc on various carbon supports[8] can enhance its CO_2RR performance by facilitating electron transfer from the carbon supports to the catalytic active sites. Recently, axial ligation of CoPc has been proven to be an alternative means to escalate the performance of CoPc. For instance, Cruz et al.[9] demonstrated that the performance of CO_2RR of axial ligands-modified CoPc is directly correlated with the σ-donor strength of the axial ligands. Although axial ligation of CoPc has been reported to be an efficient strategy to enhance its CO_2RR performance, the function of the axial ligands, especially how they influence molecule packing, electronic structure, and redox properties of CoPc, is not clear.[10]

Herein, we report an axial ligand modification strategy of CoPc to enhance the CO_2RR performance. Structural characterization demonstrates that the molecular structures of modified CoPc were shifted from the original β-phase to α-phase and clear Davydov splitting was observed in the Ultraviolet-visible (UV-vis) spectrum when imidazole was employed as the axial ligand. Additionally, the Co center electron density was depleted through π-backbonding from the filled Co d orbital to the unoccupied π* orbitals of axial ligands. Electrochemical measurements show that pyridine-modified (CoPc-py) and imidazole-modified (CoPc-im) CoPc possess an enhanced CO generation Faradaic Efficiency (FE) up to 91% (CoPc-py) and 94% (CoPc-im) compared to 82% (CoPc) at -0.82 V vs. RHE. Moreover, the current density, which indicates how fast the electrochemical reaction is, increased from 2.99 mA/cm^2 (CoPc) to 6.15 mA/cm^2 (CoPc-py) and 5.93 mA/cm^2 (CoPc-im). The structural characterization and density functional theory (DFT) calculations reveal that, firstly, axial ligation elevates the dz^2 orbital energy of

CoPc and decreases the electron density of cobalt center, leading to the one-electron reduced compounds ([CoPc-L]$^-$, L is the axial ligand) to be more nucleophilic. This facilitates the adsorption of CO_2 and improves interactions between the reduced compounds and CO_2. Additionally, the DFT calculations show the energy barrier of the rate-determining step in CO_2 activation decreased with the axial ligand modification, which further clarifies the role of axial ligand in enhancing the performance of CO_2RR.

Results and Discussion

Synthesis and Characterization

The axial ligands modified CoPc (**Figure 1a**) catalysts: CoPc-py (**Figure 1b**) and CoPc-im **(Figure 1c**) were prepared through a facile reaction by reacting CoPc and pyridine (or imidazole) to form the five-coordinated square pyramidal structure (**Supporting Information**).

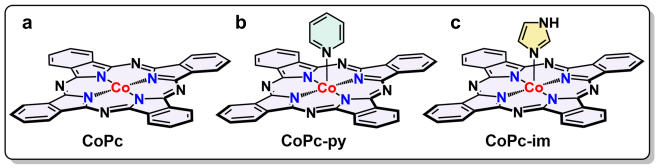

Figure 1. Proposed structures of (a) CoPc, (b) CoPc-py, and (c) CoPc-im.

CoPc powder exhibits clear diffraction peaks at 2θ = 7.108° and 2θ = 9.247° (**Figure 2a**), corresponding to the (100) and (102) crystal planes of the CoPc (**Table S1**), respectively. This indicates the presence of the β-CoPc (**Figure S1a-b,** PDF# 14-0948) crystal structure (**Table S2**), in which the adjacent columns of molecules are almost perpendicular. Characteristic peaks of α-CoPc (**Figure S1c-d,** PDF # 44-1994), such as 2θ = 16.233° and 16.703° (**Table S1**) are observed in CoPc-py and CoPc-im, respectively, which implies that incorporating the axial ligands change the preferential packing structure of CoPc.[11] UV-vis spectroscopy was used to further characterize the CoPc, CoPc-py, and CoPc-im owing to their substitute-dependent optical responses. The UV-vis spectrum of CoPc (**Figure 2b**) exhibits two characteristic peaks: a weak B band (or Soret band), resulting from the transition between deeper π orbitals to the lowest unoccupied molecular orbital (LUMO) and an intense Q band, which is attributed to the π→π* electron transition from the highest occupied molecular orbital (HOMO) to the LUMO of the phthalocyanine ring.[12] The addition of the axial ligand caused a blue shift in the CoPc Q band (from 669 nm to 660 nm for CoPc-py and CoPc-im). This indicates a decrease in the electron density of the cobalt center on CoPc, attributed to the π-backdonation from the filled d orbital of Co to a π* orbital of the axial ligand.[13] Interestingly, the Q band of CoPc-im splits into two bands, between 660 nm and 740 nm, known as Davydov splitting.[14] The Davydov splitting usually occurs from the interaction between transition dipole moments of different orientations of molecules that are adjacent to each other at a close enough distance to give electronic transitions.[15] The strong Davydov splitting indicates that axial imidazole coordination leads to a herringbone arrangement in CoPc-im.[16] The change of molecular arrangement in CoPc-py and CoPc-im as indicated by UV-vis is in good agreement with XRD results.

Fourier transform infrared spectroscopy (FTIR) further confirms the structure of CoPc-py and CoPc-im. As shown in **Figure 2c**, characteristic C=N and C-H out-of-plane bending is identified at 732 cm^{-1} in CoPc, while the similar absorption band for CoPc-py and CoPc-im is located at 724 cm^{-1}. For CoPc, the C=N in plane stretching vibration and C-H in plane deformation absorption are further identified at 780 cm^{-1} and 1086 cm^{-1}, respectively. In comparison, those two characteristic peaks in CoPc-py and CoPc-im shift to 774 cm^{-1}, 1091 cm^{-1}, 777 cm^{-1} and 1090 cm^{-1}, respectively (**Figure S3 and Table S3**). The shift of characteristic peaks further suggests that the addition of axial ligands will lead to the molecular stacking model changes. Moreover, enhanced characteristic stretches of C=N[17] and C-N[18] at 1607 and 1250 cm^{-1} are observed in CoPc-py and CoPc-im, respectively, which are ascribed to the presence of axial pyridine and imidazole on CoPc. In addition, Raman spectra (**Figure S4**) show similar peak shifts which support the FTIR results. In summary, CoPc-py and CoPc-im exhibit a near α-phase crystal structure compared to β-phase, which shows a distinguishable molecular stacking model and arrangement, as reflected in results from XRD, FTIR, and Raman spectroscopy.

The electronic effect of the axial ligand was further investigated by X-ray photoelectron spectroscopy (XPS). In the Co 2p spectrum, compared to those of prinstine CoPc, after axial-ligand modification peaks shift to higher binding energies, which indicates a decrease in electron density of the Co center (**Figure 2d**). In addition, to differentiate Co^{II} and Co^{III}, the Co $2p_{1/2}$-$2p_{3/2}$ spin-orbital energy spacing is used, where a 16.0 eV difference indicates the existence of high-spin Co^{II} whereas a 15.0 eV difference represents the presence of low-spin Co^{III}.[19] The Co $2p_{1/2}$-Co $2p_{3/2}$ spin-orbital energy spacings are 15.40 eV, 15.50 eV, and 15.10 eV in CoPc, CoPc-py and CoPc-im, respectively. These values are between 15.0 eV and 16.0 eV, indicating the coexistence of Co^{II} and Co^{III}. After the deconvolution of Co 2p XPS spectra, a higher ratio of Co^{III}/Co^{II} (**Table S4**) was observed in axial ligands-modified CoPc (CoPc-py and CoPc-im) compared to CoPc. This phenomenon indicates a reduced electron density on the Co center upon the attachment of axially anchored ligands. Meanwhile, a relatively higher percentage of Co-N_x species was observed from N 1s XPS spectra (**Figure S6 and Table S5**) in the axial ligand-coordinated samples. In addition, in CoPc-im, pyrrolic N is identified, confirming the successful coordination of axial imidazole.[20]

To further understand the local structure of CoPc-py and CoPc-im, X-ray absorption near-edge structures (XANES) and extended X-ray absorption fine structure (EXAFS) of Co were carried out. The Co K-edge XANES spectrum (**Figure 2e**) of CoPc exhibits two characteristic adsorption peaks that are the fingerprints of the Co-N_4 structure: a weak peak at 7709 eV, that is assigned to the dipole forbidden 1s to 3d transition; and a strong peak at 7716 eV, that is attributed to the 1s to $4p_z$ shakedown satellite.[10b] Compared to that of CoPc, the 1s to $4p_z$ peaks at 7716 eV are much weaker in CoPc-py and CoPc-im, which agrees with a transformation from a 4-coordinate square planar geometry

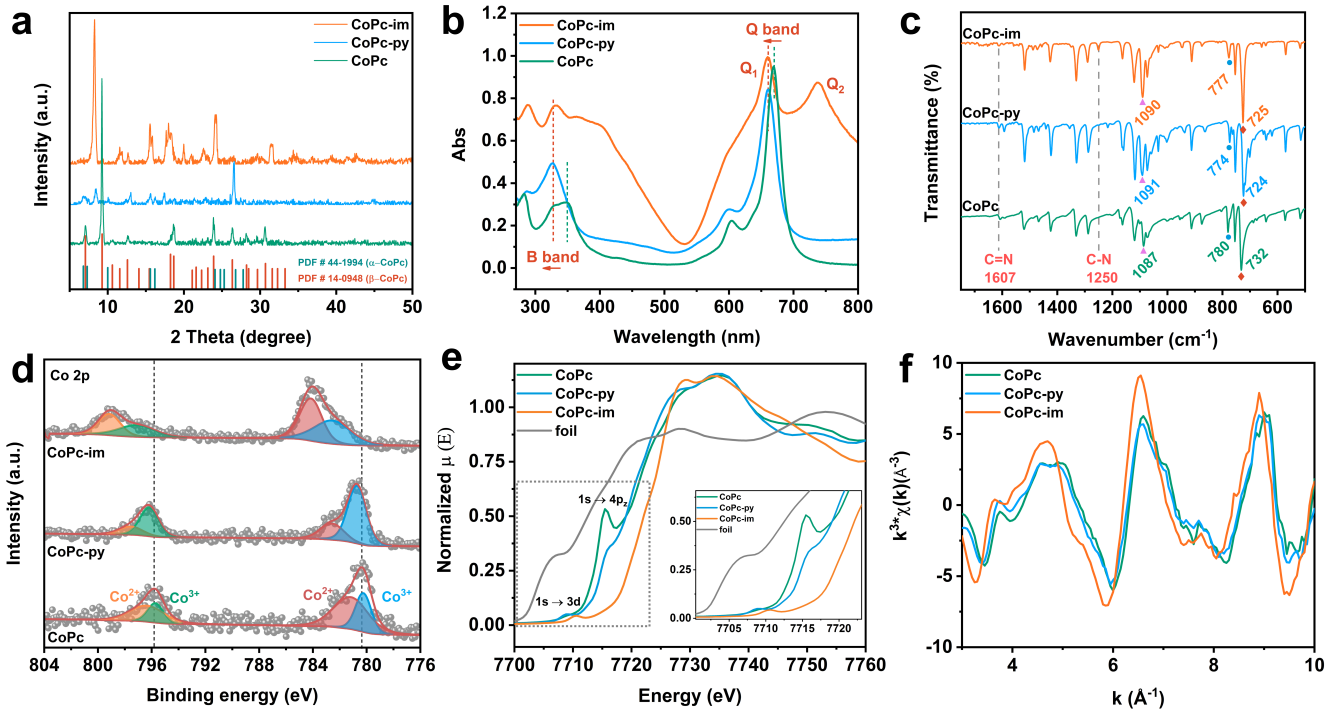

Figure 2. Structural characterizations of CoPc, CoPc-py, and CoPc-im. (a) XRD patterns. (b) UV-vis spectra in DMF with 0.05 mM concentration. (c) FTIR spectra. (d) Co 2p XPS spectra. (e) XANES spectra of Co K-edge spectra. (f) Co K edge K-space spectra.

(CoPc) to a 5-coordinate square-pyramidal structure (CoPc-py and CoPc-im).[10b] The first derivatives of the Co K-edge XANES (**Figure S7a**) confirmed the change of Co valence state in CoPc-py and CoPc-im, where more Co^{III} species were presented after coordinating with the axial ligand, consistent with the XPS results. In addition, the R distance (without phase correction) between Co and N at the first coordination sphere (Co-N_1) (1.47 Å) remained unchanged in CoPc-py and CoPc-im (**Figure S7b, Table S6**) compared to CoPc. However, the bond distances of Co-C and Co-N_2 at the second coordination sphere were reduced from 2.55 Å (CoPc) to 2.52 Å (CoPc-py and CoPc-im), and from 3.62 Å (CoPc) to 3.59 Å (CoPc-py) and 3.56 Å (CoPc-im), respectively. The decreased Co-C and Co-N_2 distances in CoPc-py and CoPc-im suggest a distortion of phthalocyanine molecule that results from coordinating with the axial ligand. The apparent difference in k-space further confirmed this transformation (**Figure 2f**). The coordination number of the Co atom in CoPc-py and CoPc-im is determined to be five via the EXAFS fitting, indicating the formation of a square-pyramidal structure. The additional axial coordination (Co-N_3) is introduced from pyridine or imidazole to the Co center (**Table S7**). These results together suggested that CoPc-py and CoPc-im with square pyramidal coordination geometries were successfully synthesized by coordinating with the axial ligands.

Electrochemical Measurements

The electrochemical properties and catalytic performance of the axial ligand-modified CoPc were accessed. Herein, cyclic voltammograms (CV) measurements were obtained in the Ar-saturated 0.5 M $KHCO_3$ (pH 8.94) (**Figure 3a and Figure S9a**). The reversible redox peak (R_1), corresponding to Co^{II}/ Co^{I}, at around E_{pc} = -0.58 V (vs. Ag/AgCl), was revealed.[21] In addition, the peak current intensity increased as a function of the scan rate. (**Figure S8**). In addition, the irreversible peak appearing at E_{pa} = -0.70 V (vs. Ag/AgCl, Ox_2), is attributed to Co^{III}/Co^{II}. Additionally, in CoPc-im, the peak present at E_{pa} = 0.79 V (vs. Ag/AgCl,, Ox_3) in the anodic scan is assigned to the oxidation of the phthalocyanine macrocycle (**Table S8**).[22] As shown in **Figure S9b**, no extra waves were observed from imidazole and pyridine CV scans, which suggests the redox peaks are from the CoPc molecules instead of the organic ligands. The enhancement of the Co^{III}/Co^{II} peak in CoPc-py and CoPc-im aligns well with the XPS results that axial ligands induce the formation of more Co^{III} species. The increased Co^{III} species in CoPc-py and CoPc-im are attributed to the cobalt-to-axial ligand π-backbonding charge transfer.

To evaluate the electrocatalytic performance of the developed catalysts, electrochemical measurements were carried out in a gas-tight H-type cell with a standard three-electrode configuration. Initially, the cyclic voltammetry (CV) was measured in 0.5 M $KHCO_3$ solution saturated with CO_2 or Ar. CV of CoPc-py and CoPc-im exhibited a broad irreversible cathodic wave (at ~ -1.50 V vs. Ag/AgCl), which is attributed to the increased catalytic activity in the presence of CO_2. In contrast, there is no peak at a similar position in the presence of Ar (**Figure 3b and Figure S10**). Linear sweep voltammetry (LSV) was also recorded in a CO_2-saturated $KHCO_3$ solution (0.5 M, pH 7.30). Compared to CoPc, enhanced cathodic current densit and positively shifted onset potentials of CoPc-py and CoPC-im (**Figure 3c**) were noticed. These results show that when CoPc is modified by axial ligands, its catalytic activity for CO_2RR is improved.

To quantify the activity and selectivity of the modified CoPc towards CO_2RR, the controlled-potential electrolysis was operated in a CO_2-saturated $KHCO_3$ solution (0.5 M, pH 7.30). First, the gas and liquid products were identified by gas chromatography (GC) and ^{1}H nuclear magnetic resonance spectroscopy (^{1}H NMR), respectively. Carbon monoxide (CO)

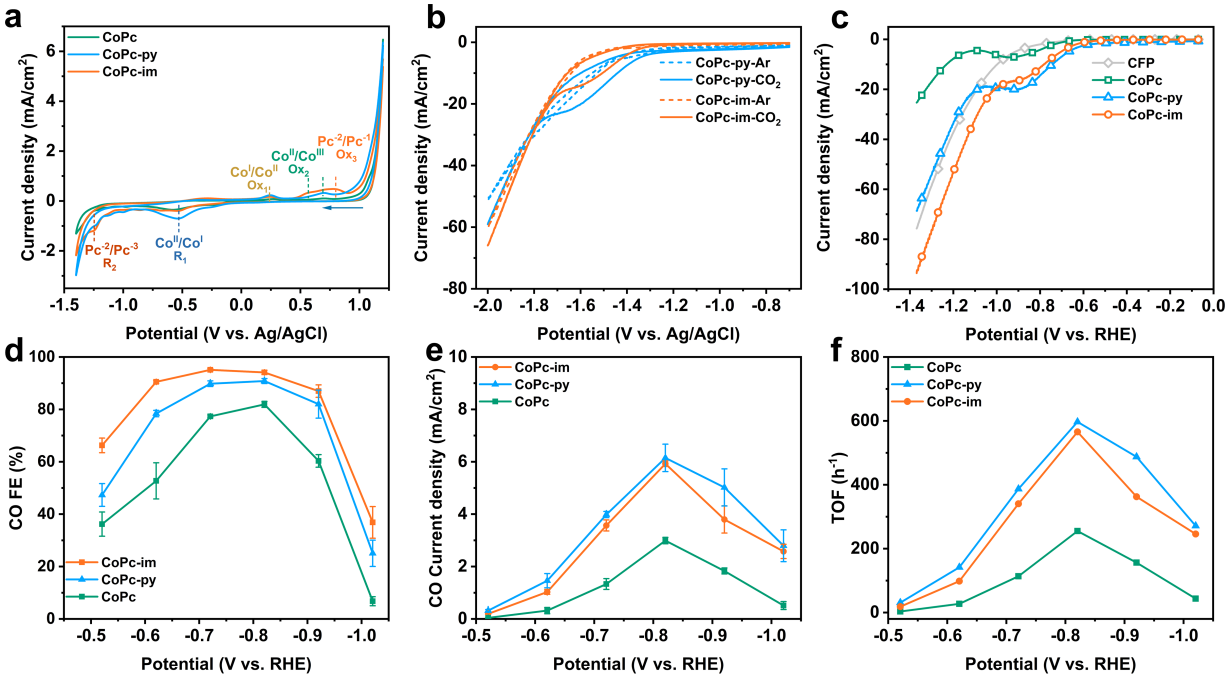

Figure 3. Electrochemical measurements of CoPc, CoPc-py, and CoPc-im. (a) CVs in Ar-saturated 0.5 M $KHCO_3$ solution at 100 mV/s. (b) CVs of CoPc-py and CoPc-im in 0.5 M $KHCO_3$ solution saturated with Ar or CO_2 at 100 mV/s. (c) LSVs in CO_2-saturated 0.5 M $KHCO_3$ solution at 5 mV/s. (d) FEs of CO. (e) Current densities of CO. (f) Corresponding TOF numbers for CO. When the error bars are presented, data is represented as mean ± standard deviation of at least 3 individual experiments.

was identified as the major product, accompanied by H_2 as the byproduct. In addition, no liquid products were detected, as confirmed by the ^1H NMR (**Figure S11**). The FE of CO and the current density (**Figure 3d, 3e**) showed escalated values on CoPc-py and CoPc-im compared to CoPc in the potential range from -0.52 V to -1.02 V. For CoPc catalysts, the optimal FE of 82 ± 1.2% was obtained at -0.82 V vs. RHE. At the same potential, CoPc-py and CoPc-im exhibited enhancements of FE which were 91 ± 0.9% and 94 ± 0.8%, respectively. Moreover, CoPc-py and CoPc-im could achieve about twice the CO current densities of 6.15 mA/cm^2 and 5.93 mA/cm^2, respectively, relative to the 2.99 mA/cm^2 current density of CoPc. Meanwhile, the turnover frequency (TOF) for CO was calculated based on the total moles of molecular catalysts immobilized on carbon fiber paper (CFP). It is worth noting that in this work, the active sites were not quantified by integrating the CV peak for Co^{II} to Co^{I}, due to difficulty in accessing an accuracy result from the low loading amount of catalysts on CFP. The TOFs for CO production of CoPc-py and CoPc-im was calculated to be 597 h^{-1} and 565 h^{-1}, respectively, which was approximately 2.3 times higher than that of CoPc (255 h^{-1}) at -0.82 V (**Figure 3f**). Additionally, CoPc-py and CoPc-im exhibit higher electrochemical active surface area (ECSA) than that of CoPc, which is directly proportional to an increase double-layer capacitance (C_{dl}) as shown in **Figure S13 and S14a**. The ECSA-normalized CO partial current density was demonstrated in **Figure S14b**. Lastly, stability is an important criterion to describe the performance of CO_2RR catalysts. To determine the stability of CoPc-py and CoPc-im, long-term electrolysis at the potential of -0.82 V vs. RHE (**Figure S16**) was conducted. Both CoPc-py and CoPc-im showed stable current densities with small decays for around 5 h and FEs remained above 90%, indicating that both catalysts have excellent durability under these operating conditions. Meanwhile, Co 2p XPS spectra were further performed to investigate the stability. As shown in Co 2p XPS spectra (**Figure 17)**, after electrolysis (-0.82 V vs. RHE) for 5 hours, Co 2p spectra of CoPc-py and CoPc-im exhibit 0.43 eV and 0.61 eV binding energy shift compared to bare CoPc, respectively. The positive binding energy shift of Co center indicates the presence of axial ligands after long-term electrolysis. However, compared to the original CoPc-py and CoPc-im, after long-term electrolysis, the binding energy shift of CoPc-py (or CoPc-im) versus CoPc becomes smaller, which suggests the axial ligands partial dissociation during the CO_2RR, agreeing well with the current density decay in the stability tests.

From CV analyses of CoPc-py and CoPc-im, the Co^{III}/Co^{II} peaks (at 0.70 V and 0.57 V vs. Ag/AgCl for CoPc-py and CoPc-im, respectively) were found to be irreversible (**Figure 3a**). In addition, the redox peaks of Co^{II}/Co^{I} (at ~0.20 V vs. RHE) can be identified when scanning from the anodic direction. This result, together with previously reported work,[8b, 23] strongly suggests that the catalytic reaction was triggered by the reduction of Co^{II} to Co^{I} in all samples even though CoPc-py and CoPc-im contain more Co^{III} species. Therefore, one-electron reduced CoPc-L is the active species for CO_2RR (**Scheme 1**).

Density Functional Theory Calculations

Further, DFT calculations were employed to investigate the relative free energies and molecular orbitals of the metal complexes before (neutral form) and after one-electron reduction. In the neutral form (**Table S10**), the dz^2 orbital is found to be the HOMO-14 orbital in CoPc (Co^{II} d^7). In contrast, the dz^2 becomes the LUMO in CoPc-py and CoPc-im, because the Co center donates electrons to an axial ligand π* orbital through π-back

donation, leading to the formation of more Co^{III} (Co d^6) species. In the one-electron reduced form ([CoPc-L]$^-$, **Figure 4a and Table S11**), the dz^2 orbital in CoPc occupies relatively lower energy (HOMO-12) compared to the ligated compounds. Upon axial ligation, the dz^2 orbital is elevated to HOMO-1 in CoPc-py and CoPc-im. At the same time, the Co center coordination geometry changes from square planar to square pyramidal. Hypothetically, the elevated dz^2 orbital energy in CoPc-L leads to easier electron delocalization from the Co $3dz^2$ orbital to the CO_2 π* orbital, increasing the nucleophilicity on the Co center and enhancing the Co center's ability to coordinate and activate the Lewis carbon on experimental observations that CoPc-py and CoPc-im are more efficient and selective than pristine CoPc. The optimized structures of all three catalysts for each CO_2 reduction step were displayed in **Figure S18a-c**. The results of DFT calculation confirm that the elevation energetics of the dz^2 orbital via axial ligation can decrease the CO_2 reduction RDS energy barrier, facilitating the formation of *COOH intermediate. This result correlated well with the hypothesis that coordination with the axial ligand would increase the nucleophilicity of the Co center.

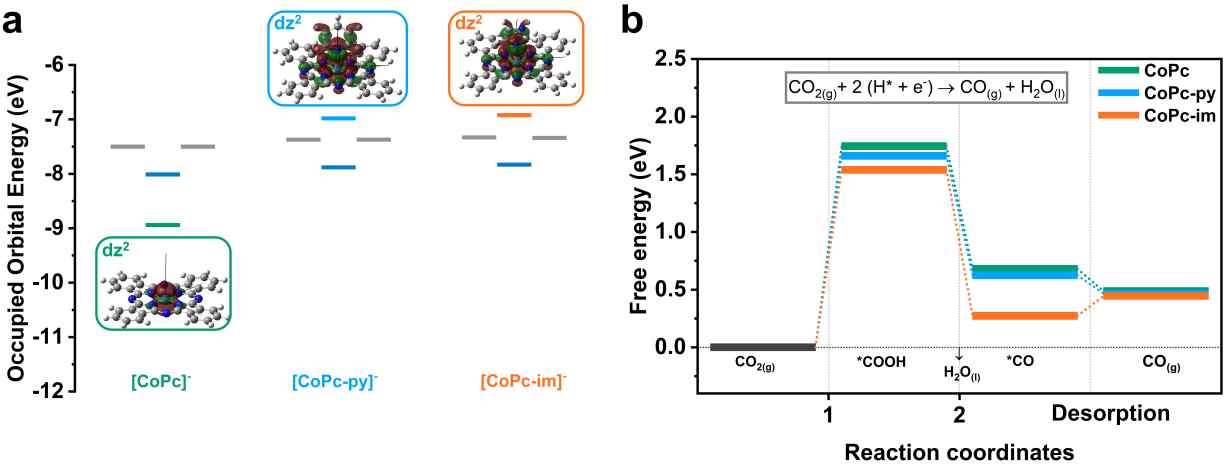

Figure 4. (a) Occupied molecular orbitals for one-electron reduced form of [CoPc]$^-$, [CoPc-py]$^-$ and [CoPc-im]$^-$. Graphical representation of the dz^2 orbital with color labels for different molecules are shown. The colors of energy level correspond to the specific molecular orbitals: blue is d_{xy}, gray is d_{xz} and d_{yz}. Summaries of the orbital energies and assignments are shown in **Table S10** and **Table S11**. (b) Free energy diagram of $CO_{2(g)}$ electroreduction to $CO_{(g)}$ on CoPc, CoPc-py, and CoPc-im. All energies are referred to $CO_{2(g)}$ and proton-electron pairs.

CO_2.[10a] It is expected that the enhanced interaction between the Co center and CO_2 lowers the activation energy barrier for converting CO_2 into CO. Additionally, the Co center electron density is reduced through Co to axial ligand π-back donation after axial ligation; therefore, the Co-CO π-backbonding is weakened, resulting in rapid CO desorption. To confirm this hypothesis, we have also calculated the energetics of the intermediate reaction pathways (**Computational Methods in Support Information**). The formation of *COOH is assumed to be the rate-determining step (RDS) for all catalysts because the formation of *COOH intermediates is the most endergonic step. As shown in **Figure 4b**, the required free energy change from CO_2 to the adsorbed *COOH for CoPc-py and CoPc-im is 1.66 eV and 1.54 eV, respectively, lower than that of CoPc (1.74 eV), confirming the beneficial energetics in modifying CoPc with an axial ligand. In addition, after forming adsorbed *COOH, for the second proton-coupled electron-transfer step, the free energy pathway was thermodynamically downhill to form the adsorbed *CO. While CoPc-im still needs to overcome an energy barrier (0.3 eV) for *CO desorption, its *CO desorption process is endergonic compared to the exothermic process of CoPc-py and CoPc, suggesting the CoPc-im catalyst might be sensitive to be poisoning by strong CO adsorption.[24] This phenomenon might be attributed to the stronger π acceptor strength of pyridine compared with imidazole, which reduces Co-CO π* orbital back donation. Overall, the RDS energy barriers of CO_2RR on CoPc-py and CoPc-im are much lower than that of CoPc, explaining our

Conclusion

In summary, we reported an efficient axial ligation strategy with pyridine and imidazole to modify CoPc's coordination environment, enhancing its electrochemical CO_2-to-CO performance. XRD and FTIR show a clear phase change of CoPc from β-phase to near α-phase, and stronger Davydov splitting of the Q band is observed in UV-vis spectra after axial ligation. XAS fitting results indicate the formation of the square-pyramidal structure after pyridine and imidazole axially coordinate with CoPc. XPS spectra elucidate a clear binding energy shift on Co 2p orbital, suggesting the existence of a π-backbonding effect from Co center filled d orbital to ligand π* orbital. In CO_2RR experiments, CoPc-py and CoPc-im achieved an enhanced FE and current density of CO, up to 91% (6.15 mA/cm^2) and 94% (5.93 mA/cm^2) in comparison with 82% (2.99 mA/cm^2) of CoPc, respectively. DFT calculations confirmed that the dz^2 energy was elevated at the Co center in the axial ligand modified CoPc. The dz^2 energy elevation is the origin of the improved CO_2RR since it significantly decreases the formation energy of *COOH intermediates. In addition, comparing CoPc-py to CoPc, the stronger π-backbonding from the Co center to the axial ligands can weaken the Co-CO bond, which is beneficial to CO desorption, while CoPc-im catalyst might be sensitive to be poisoining by strong CO adsorption. This work demonstrates the importance of axial

direction modification of molecular catalysts, providing an alternative strategy to modify transition metal macrocycles (e.g., porphyrin, corrole, phthalocyanine, and so on) complexes for more efficient CO_2 electrochemical conversion.

Experimental Section

Synthesis of CoPc-py: 80 mg cobalt (II) phthalocyanine (CoPc) was put into a round-bottom flask and heated at 135 ºC for 3 hours under a reduced pressure in oil-bath with stirring to remove moisture. After the CoPc solid was cooled down to 75 ºC, the solution of 5 ml pyridine in 10 ml N,N-Dimethylformamide was added into flask. Subsequently, the mixed solution was heated at 75 ºC for 24 hours. After cooling down to room temperature, the mixture was centrifuged, in which the precipitate was washed with ethanol five times to remove the unreacted starting chemicals. Finally, the precipitate, denoted as CoPc-py (py refers to pyridine) was dried at 60 ºC in a vacuum oven for 24 hours.

Synthesis of CoPc-im: CoPc-im was synthesized using a similar procedure as for CoPc-py with imidazole (81 mg) as the precursor. The large excess of axial ligands was added in the synthesis to ensure that equilibrium would favor the formation of axial ligand coordinated metal complex.

Supporting Information

Additional references cited within the Supporting Information.[25-42]

Acknowledgements

J. Gu acknowledges the financial support received for this research from NSF award CHE-2154837. A.L. Cooksy acknowledges research support from NSF XSEDE allocation CHE-210058.

Conflict of Interest

The authors declare no conflict of interest.

Data Availability Statement

The data that support the findings of this study are available in the supplementary material of this article.

Keywords: Cobalt phthalocyanine, CO_2 reduction reaction, axial ligation, π-backbonding

[1] a) W. Wang, S. Wang, X. Ma, J. Gong, *Chem. Soc. Rev.* **2011**, *40*, 3703-3727; b) T. P. Senftle, E. A. Carter, *Acc. Chem. Res.* **2017**, *50*, 472-475; c) P. De Luna, C. Hahn, D. Higgins, S. A. Jaffer, T. F. Jaramillo, E. H. Sargent, *Science* **2019**, *364*, eaav3506.

[2] a) S. Nitopi, E. Bertheussen, S. B. Scott, X. Liu, A. K. Engstfeld, S. Horch, B. Seger, I. E. L. Stephens, K. Chan, C. Hahn, J. K. Norskov, T. F. Jaramillo, I. Chorkendorff, *Chem. Rev.* **2019**, *119*, 7610-7672; b) H. Shen, T. Peppel, J. Strunk, Z. Sun, *Sol. RRL* **2020**, *4*, 1900546.

[3] a) M. B. Ross, P. De Luna, Y. Li, C.-T. Dinh, D. Kim, P. Yang, E. H. Sargent, *Nat. Catal.* **2019**, *2*, 648-658; b) D. H. Nam, P. De Luna, A. Rosas-Hernandez, A. Thevenon, F. Li, T. Agapie, J. C. Peters, O. Shekhah, M. Eddaoudi, E. H. Sargent, *Nat. Mater.* **2020**, *19*, 266-276.

[4] a) A. Call, M. Cibian, K. Yamamoto, T. Nakazono, K. Yamauchi, K. Sakai, *ACS Catal.* **2019**, *9*, 4867-4874; b) E. Boutin, L. Merakeb, B. Ma, B. Boudy, M. Wang, J. Bonin, E. Anxolabehere-Mallart, M. Robert, *Chem. Soc. Rev.* **2020**, *49*, 5772-5809.

[5] a) X. Zhang, Y. Wang, M. Gu, M. Wang, Z. Zhang, W. Pan, Z. Jiang, H. Zheng, M. Lucero, H. Wang, G. E. Sterbinsky, Q. Ma, Y.-G. Wang, Z. Feng, J. Li, H. Dai, Y. Liang, *Nat. Energy* **2020**, *5*, 684-692; b) Z. Weng, Y. Wu, M. Wang, J. Jiang, K. Yang, S. Huo, X. F. Wang, Q. Ma, G. W. Brudvig, V. S. Batista, Y. Liang, Z. Feng, H. Wang, *Nat. Commun.* **2018**, *9*, 415.

[6] Z. Zhang, J. Xiao, X. J. Chen, S. Yu, L. Yu, R. Si, Y. Wang, S. Wang, X. Meng, Y. Wang, Z. Q. Tian, D. Deng, *Angew Chem. Int. Ed.* **2018**, *57*, 16339-16342.

[7] a) X. Zhang, Z. Wu, X. Zhang, L. Li, Y. Li, H. Xu, X. Li, X. Yu, Z. Zhang, Y. Liang, H. Wang, *Nat. Commun.* **2017**, *8*, 14675; b) Y. Wu, Z. Jiang, X. Lu, Y. Liang, H. Wang, *Nature* **2019**, *575*, 639-642; c) M. Wang, K. Torbensen, D. Salvatore, S. Ren, D. Joulie, F. Dumoulin, D. Mendoza, B. Lassalle-Kaiser, U. Isci, C. P. Berlinguette, M. Robert, *Nat. Commun.* **2019**, *10*, 3602.

[8] a) X. M. Hu, M. H. Ronne, S. U. Pedersen, T. Skrydstrup, K. Daasbjerg, *Angew. Chem. Int. Ed.* **2017**, *56*, 6468-6472; b) M. Zhu, R. Ye, K. Jin, N. Lazouski, K. Manthiram, *ACS Energy Lett.* **2018**, *3*, 1381-1386; c) J. Choi, P. Wagner, S. Gambhir, R. Jalili, D. R. MacFarlane, G. G. Wallace, D. L. Officer, *ACS Energy Lett.* **2019**, *4*, 666-672; d) H. Gu, L. Zhong, G. Shi, J. Li, K. Yu, J. Li, S. Zhang, C. Zhu, S. Chen, C. Yang, Y. Kong, C. Chen, S. Li, J. Zhang, L. Zhang, *J. Am. Chem. Soc.* **2021**, *143*, 8679-8688; e) X. Wu, J. W. Sun, P. F. Liu, J. Y. Zhao, Y. Liu, L. Guo, S. Dai, H. G. Yang, H. Zhao, *Adv. Funct. Mater.* **2021**, *32*, 2107301.

[9] K. E. Rivera Cruz, Y. Liu, T. L. Soucy, P. M. Zimmerman, C. C. L. McCrory, *ACS Catal.* **2021**, *11*, 13203-13216.

[10] a) W. W. Kramer, C. C. L. McCrory, *Chem. Sci.* **2016**, *7*, 2506-2515; b) Y. Liu, A. Deb, K. Y. Leung, W. Nie, W. S. Dean, J. E. Penner-Hahn, C. C. L. McCrory, *Dalton Trans.* **2020**, *49*, 16329-16339.

[11] a) X. Ji, T. Zou, H. Gong, Q. Wu, Z. Qiao, W. Wu, H. Wang, *Cryst. Res. Technol.* **2016**, *51*, 154-159; b) Y. Xiao, L. Zhang, F. Peng, G. B. Pan, *RSC Adv.* **2018**, *8*, 5344-5349.

[12] a) N. Han, Y. Wang, L. Ma, J. Wen, J. Li, H. Zheng, K. Nie, X. Wang, F. Zhao, Y. Li, J. Fan, J. Zhong, T. Wu, D. J. Miller, J. Lu, S.-T. Lee, Y. Li, *Chem* **2017**, *3*, 652-664; b) A. N. Andriianova, A. G. Mustafin, I. B. Abdrakhmanov, *ChemistrySelect* **2019**, *4*, 11307-11314.

[13] F. Tessore, G. Di Carlo, A. Forni, S. Righetto, F. Limosani, A. Orbelli Biroli, *Inorganics* **2020**, *8*.

[14] R. R. Cranston, B. H. Lessard, *RSC Adv.* **2021**, *11*, 21716-21737.

[15] a) S. Karan, D. Basak, B. Mallik, *Chem. Phys. Lett.* **2007**, *434*, 265-270; b) S. K. a. B. Mallik, *J. Phys. Chem. C* **2008**, *112*, 2436-2447.

[16] H. L. a. N. B. M. Bashir M. Hassan, *J. Mater. Chem.* **1999**, *10*, 39-45.

[17] a) A. Penkova, L. F. Bobadilla, F. Romero-Sarria, M. A. Centeno, J. A. Odriozola, *Appl. Surf. Sci.* **2014**, *317*, 241-251; b) J. J. Gabla, S. R. Mistry, K. C. Maheria, *Catal. Sci. Technol.* **2017**, *7*, 5154-5167; c) R. Wang, X. Wang, W. Weng, Y. Yao, P. Kidkhunthod, C. Wang, Y. Hou, J. Guo, *Angew. Chem. Int. Ed.* **2022**, *61*, e202115503.

[18] a) J. Huang, Q. Lu, X. Ma, X. Yang, *J. Mater. Chem. A* **2018**, *6*, 18488-18497; b) K. Li, L. Qian, W. Song, M. Zhu, Y. Zhao, Z. Miao, *J Mater. Sci.* **2018**, *53*, 14821-14833.

[19] a) M. O. a. K. Hirokawa, *J. Electron Spectrosc. Relat. Phenom.* **1976**, *8*, 475-481; b) M. Zhu, J. Chen, L. Huang, R. Ye, J. Xu, Y. F. Han, *Angew. Chem. Int. Ed.* **2019**, *58*, 6595-6599.

[20] a) D. Y. Osadchii, A. I. Olivos-Suarez, A. V. Bavykina, J. Gascon, *Langmuir* **2017**, *33*, 14278-14285; b) W. He, R. Ifraemov, A. Raslin, I. Hod, *Adv. Funct. Mater.* **2018**, *28*.

[21] I. S. Hosu, Q. Wang, A. Vasilescu, S. F. Peteu, V. Raditoiu, S. Railian, V. Zaitsev, K. Turcheniuk, Q. Wang, M. Li, R. Boukherroub, S. Szunerits, *RSC Adv.* **2015**, *5*, 1474-1484.

[22] F. Aytan Kiliçarslan, B. Keskin, İ. Erden, A. Erdoğmuş, *J. Coord. Chem.* **2017**, *70*, 2671-2683.
[23] Y. Liu, C. C. L. McCrory, *Nat. Commun.* **2019**, *10*, 1683.
[24] a) S. Fernández, F. Franco, C. Casadevall, V. Martin-Diaconescu, J. M. Luis, J. Lloret-Fillol, *J. Am. Chem. Soc.* **2020**, *142*, 120-133; b) X. Lu, B. Dereli, T. Shinagawa, M. Eddaoudi, L. Cavallo, K. Takanabe, *Chem Catal.* **2022**, *2*, 1143-1162.
[25] a) M. J. T. Frisch, G. W.; Schlegel, H. B.; Scuseria, G. E.; Robb, M. A.; Cheeseman, J. R.; Scalmani, G.; Barone, V.; Petersson, G. A.; Nakatsuji, H.; Li, X.; Caricato, M.; Marenich, A. V.; Bloino, J.; Janesko, B. G.; Gomperts, R.; Mennucci, B.; Hratchian, H. P.; Ortiz, J. V.; Izmaylov, A. F.; Sonnenberg, J. L.; Williams; Ding, F.; Lipparini, F.; Egidi, F.; Goings, J.; Peng, B.; Petrone, A.; Henderson, T.; Ranasinghe, D.; Zakrzewski, V. G.; Gao, J.; Rega, N.; Zheng, G.; Liang, W.; Hada, M.; Ehara, M.; Toyota, K.; Fukuda, R.; Hasegawa, J.; Ishida, M.; Nakajima, T.; Honda, Y.; Kitao, O.; Nakai, H.; Vreven, T.; Throssell, K.; Montgomery Jr., J. A.; Peralta, J. E.; Ogliaro, F.; Bearpark, M. J.; Heyd, J. J.; Brothers, E. N.; Kudin, K. N.; Staroverov, V. N.; Keith, T. A.; Kobayashi, R.; Normand, J.; Raghavachari, K.; Rendell, A. P.; Burant, J. C.; Iyengar, S. S.; Tomasi, J.; Cossi, M.; Millam, J. M.; Klene, M.; Adamo, C.; Cammi, R.; Ochterski, J. W.; Martin, R. L.; Morokuma, K.; Farkas, O.; Foresman, J. B.; Fox, D. J. Wallingford, CT, **2016**; b) R. K. Dennington, Todd A.; Millam, John M. Semichem Inc., Shawnee Mission, KS, **2016**.
[26] a) A. D. Becke, *Phys. Rev. A. Gen. Phys.* **1988**, *38*, 3098-3100; b) A. D. Becke, *J. Chem. Phys.* **1993**, *98*, 1372-1377; c) C. Lee, W. Yang, R. G. Parr, *Phys. Rev. B. Condens. Matter.* **1988**, *37*, 785-789.
[27] S. Chiodo, N. Russo, E. Sicilia, *J. Chem. Phys.* **2006**, *125*, 104107.
[28] a) T. H. Dunning, *J. Chem. Phys.* **1989**, *90*, 1007-1023; b) K. A. Peterson, D. Figgen, M. Dolg, H. Stoll, *J. Chem. Phys.* **2007**, *126*, 124101.
[29] a) Y. Zhao, D. G. Truhlar, *Theor. Chem. Acc.* **2007**, *120*, 215-241; b) S. Grimme, J. Antony, S. Ehrlich, H. Krieg, *J. Chem. Phys.* **2010**, *132*, 154104.
[30] G. Scalmani, M. J. Frisch, *J. Chem. Phys.* **2010**, *132*, 114110.
[31] a) J. P. F. a. F. Weinhold, *J. Am. Chem. Soc.* **1980**, *102*, 7211-7218; b) F. a. C. Weinhold, John E, in *The Structure of Small Molecules and Ion* (Ed.: R. a. V. Naaman, Zeev), Springer US, Boston, MA, **1988**, pp. 227–236.
[32] R. F. W. Bader, *Atoms in Molecules: A Quantum Theory,* Oxford University Press, Oxford, **1994**.
[33] T. Lu, F. Chen, *J. Comput. Chem.* **2012**, *33*, 580-592.
[34] a) P. A. Reynolds, B. N. Figgis, E. S. Kucharski, S. A. Mason, *Acta. Crystallogr. B. Struct. Sci. Cryst. Eng. Mater.* **1991**, *47*, 899-904; b) P. Ballirano, R. Caminiti, C. Ercolani, A. Maras, M. A. Orrù, *J. Am. Chem. Soc.* **1998**, *120*, 12798-12807.
[35] a) A. Egeberg, L. Warmuth, S. Riegsinger, D. Gerthsen, C. Feldmann, *Chem. Commun. (Camb)* **2018**, *54*, 9957-9960; b) S. M. Jingxian Yu, Benjamin S. Flavel, Martin R. Johnston, and Joe G. Shapter, *J. Am. Chem. Soc.* **2008**, *130*, 8788-8796.
[36] L. A. Ahmadi, Ebrahim Mohamadnia, Zahra, *Polym. Adv. Technol.* **2021**, *32*, 3421-3435.
[37] D. D. Klyamer, T. V. Basova, P. O. Krasnov, A. S. Sukhikh, *J. Mol. Struct.* **2019**, *1189*, 73-80.
[38] a) M. Szybowicz, W. Bała, K. Fabisiak, K. Paprocki, M. Drozdowski, *Cryst. Res. Technol.* **2010**, *45*, 1265-1271; b) A. Kumar, N. Joshi, S. Samanta, A. Singh, A. K. Debnath, A. K. Chauhan, M. Roy, R. Prasad, K. Roy, M. M. Chehimi, D. K. Aswal, S. K. Gupta, *Sens. and Actuators B: Chem.* **2015**, *206*, 653-662.
[39] F. Evangelista, A. Ruocco, R. Gotter, A. Cossaro, L. Floreano, A. Morgante, F. Crispoldi, M. G. Betti, C. Mariani, *J Chem Phys* **2009**, *131*, 174710.
[40] R. Patil J. Brach, and Hugh A. Six, Webster, *United States Patent* **1973**, *3708292*.
[41] F. Aytan Kiliçarslan, B. Keskin, İ. Erden, A. Erdoğmuş, *J. Coord. Chem.* **2017**, *70*, 2671-2683.
[42] a) M. Zhu, R. Ye, K. Jin, N. Lazouski, K. Manthiram, *ACS Energy Lett.* **2018**, *3*, 1381-1386; b) Z. Meng, J. Luo, W. Li, K. A. Mirica, *J. Am. Chem. Soc.* **2020**, *142*, 21656-21669.

10.1002/cctc.202300576

WILEY-VCH

RESEARCH ARTICLE

Entry for the Table of Contents

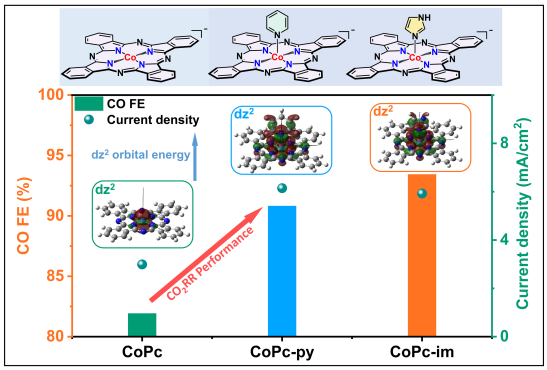

In this work, an axial coordination strategy on CoPc molecular catalyst was employed to enhance the performance of CO_2 reduction (CO_2RR). The axial ligation elevates dz^2 orbital energy and reduces the key step activation energy barrier. This work demonstrates the importance to change the coordination environments, electronic, and structure properties of transition metal macrocycles for more efficient CO_2RR.